Research Article

# Aluminum Foil Anodes for Li-Ion Rechargeable Batteries: the Role of Li Solubility within β-LiAl

Tianye Zheng, Dominik Kramer, Reiner Mönig, and Steven T. Boles*

Read Online

ACCESS | Metrics & More | Article Recommendations | Supporting Information

**ABSTRACT:** Lithium-ion battery electrodes contain a substantial amount of electrochemically inactive materials, including binders, conductive agents, and current collectors. These extra components significantly dilute the specific capacity of whole electrodes and thus have led to efforts to utilize foils, for example, Al, as the sole anode material. Interestingly, the literature has many reports of fast degradation of Al electrodes, where less than a dozen cycles can be achieved. However, in some studies, Al anodes demonstrate stable cycling life with several hundred cycles. In this work, we present a successful pathway for enabling long-term cycling of simple Al foil anodes: the β-LiAl phase grown from Al foil (α-Al) exhibits a



cycling life of 500 cycles with a ∼96% capacity retention when paired with a commercial cathode. The excellent performance stems from strategic utilization of the Li solubility range of β-LiAl that can be (de-)lithiated without altering its crystal structure. This solubility range at room temperature is determined to be ∼6 at %. Consequently, this design circumvents the critical issues associated with the α/β/α phase transformations, such as volume change, mechanical strain, and formation of nanopores. Application-wise, the maturity of the aluminum industry, combined with excellent sustainability prospects, makes this anode an important option for future devices.

**KEYWORDS:** lithium-ion battery, solid-state anode, aluminum foil, β-LiAl, solubility range
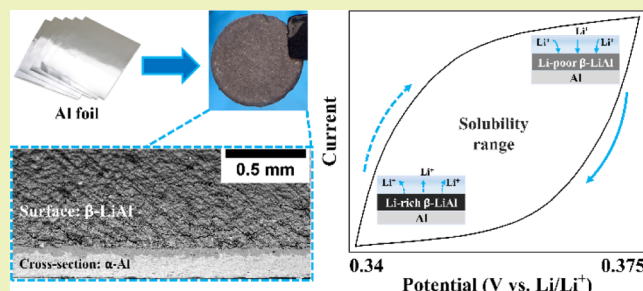
## INTRODUCTION

Aluminum has been explored as a candidate for the negative electrode in lithium-based rechargeable batteries since the 1970s.[1] Generally, investigations of this system center around the phase transformations between the α phase (fcc, Al) and the β phase (cubic, LiAl), which correspond to a high theoretical capacity of ∼993 mA h g$^{-1}$ at room temperature. Efforts were made to utilize and to understand this Li−Al electrode until Sony introduced Li-ion batteries (LIBs) with graphite as the negative electrode in the early 1990s.[2,3] During the past decade, there has been a strong shift of focus on alloy anode candidates which achieve some of the highest absolute specific capacity figures, such as silicon (Si), tin (Sn), and germanium (Ge).[4,5] To date, only limited success has been attained for Al-based anodes due to the issues that are not yet resolved, including significant mechanical strain,[6] brittleness of the β-LiAl,[7,8] and electrode pulverization during delithiation.[9,10] Our previous study suggests that the Al/LiAl/Al (α/β/α) phase transformations might be intrinsically challenging to utilize due to the formation of nanopores, which cause a loss of electrolyte due to secondary solid electrolyte interphase (SEI) formation on a large surface area. Therefore, a strategic pathway is required to mitigate degradation.[9]

From a more holistic perspective, conventional composite anodes may be ill-suited to widespread energy storage efforts if cradle-to-grave costs and sustainability are considered. In today's state-of-the-art devices, both the cathode and the anode consist of composites of active materials, polymer binders, and conductive additives. These components are dispersed into a solvent to form a "slurry", which is then pasted on the current collectors (e.g., copper foil for the anodes) for drying. Not only does the toxicity of some chemicals present risks for occupational safety and the environment but also the multi-step nature of electrode manufacturing requires significant labor and capital at scale. Similarly, the complexity of recycling and disposal increases as the mixing of materials in cells becomes increasingly significant. This electrode architecture also reduces the specific capacity, particularly because the copper current collector is electrochemically inactive, yet has a relatively high density as a material.[11] This mass of the copper current collector is often neglected in academic discussions, and numbers reported for "high-performance"

anode materials are usually normalized to the active material only.[12]

In this study, a novel anode structure has been developed by partly lithiating a metallic Al foil to form a monolithic electrode. Although this prelithiation step is performed electrochemically here, other methods like simple mechanical rolling will also be sufficient to fabricate such an electrode.[13] The $\beta$-LiAl and the $\alpha$-Al layers function as the active material and the current collector, respectively. This design significantly simplifies electrode manufacturing and reduces fabrication costs by omitting the usage of copper foils and binders. Replacing the graphite anode with such an Al-based electrode may result in a considerable reduction in material costs for LIBs because the costs of conventional copper and carbon-based anodes are roughly one-fifth the cell costs.[14] Consequently, the baking and calendering processes needed for conventional composite electrode coatings, which can be quite resource-consuming (e.g., energy/yield), are also omitted. Finally, the metallurgical nature of this electrode design may potentially have a positive impact on the sustainability prospects of such batteries as the composite nature of waste cells is reduced or eliminated.

To enable the $\beta$-LiAl on Al layered structures as a stable anode, a new concept for cycling the $\beta$-LiAl solely within its Li solubility range and without a phase transition (i.e., maintaining the $\beta$ phase crystal structure) is further proposed. Although a Li solubility range within the $\beta$ phase regime is included in the Li−Al phase diagrams, the solubility range accessible at low temperatures has never been specified due to the experimental conditions of previous phase diagram studies made above 400 °C. Different extrapolations to room temperature have been suggested, ranging from 9.2% at 423 °C, which might be maintained at room temperature,[15] to a solubility range that decreases with temperature, being less than one percent (ca. 49.2% to 50.1 at % Li) below 100 °C.[16] To the best of our knowledge, no study has determined the solubility range at room temperature and the related capacity. For electrochemical lithiation of Al, the vast majority of studies focus on $\beta$-LiAl and neglect the phases with higher Li contents because these phases necessitate very low potentials and elevated temperatures.[17] Therefore, it is believed that $\beta$-LiAl is the only relevant phase based on the first cycle capacity and X-ray data, even though trace amounts of Li-rich phases may exist, for example, on the electrode surface.[18]

Only few studies have demonstrated reasonable cycling performance for Al-based anodes, for example, a demonstration of 250 cycles with >80% capacity retention.[19] Others have found that mechanical strain caused by (de-)alloying with Li is problematic for Al anodes and the capacity loss can be limited to less than 12% after 200 cycles for a full cell paired with a LiFePO$_4$ (LFP) cathode by uniformly distributing the mechanical stress generated during (de-)lithiation.[20] Similarly, Li et al. claim that a mechanically hard Al foil can minimize the mechanical damage during the phase transition, thus giving 120 stable cycles when paired with a LiCoO$_2$ (LCO) cathode.[21] Although a mechanically stable structure can indeed contribute to the above-reported cycling performances, other beneficial aspects should not be neglected, such as material and interface chemistries. At the end of the day, a unified understanding of why Al foil anodes often fail prematurely but sometimes appear to be adequate is still yet to be achieved.

In this work, multiple approaches have been utilized to characterize the solubility range of $\beta$-LiAl independently, including electrochemical characterizations, ex situ X-ray diffraction (XRD), and in situ stress measurements. In addition, scanning electron microscopy (SEM) has been performed to observe the morphologies of partly lithiated Al foils, providing insights into the Li−Al system. Based on these observations, it is possible to electrochemically cycle the electrode such that the active layer (i.e., $\beta$-LiAl) of the anode stays within its Li solubility range. Extending the cycled amount of lithium leads to phase boundary motion between alpha and beta and can largely explain the origins of capacity fading in Al-based anodes. Finally, a full cell is assembled combining $\beta$-LiAl grown on Al and a commercially available cathode to demonstrate the feasibility of this solid-state anode technology.

## ■ EXPERIMENTAL SECTION

**Electrochemical Tests.** All electrochemical tests were carried out using a compactstat (Ivium Technologies, the Netherlands) and a VMP potentiostat (Biologic Technologies, France), including chronoamperometry (CA), galvanostatic charge−discharge (GCD), cyclic voltammetry (CV), and electrochemical impedance spectroscopy. First, the charge counting experiment (i.e., CA) was performed using 0.25 mm-thick high-purity Al foils (99.9995%; Alfa Aesar). Swagelok-type cells (Ø = 11 mm) were assembled using Al foils and Li foils as the working and the counter electrodes, respectively. A LiPF$_6$ electrolyte (1 M; EC/EMC 3:7 vol %) and a glass fiber separator (Whatman) were also utilized to achieve the typical half-cell configuration. Second, a typical cyclic voltammogram was obtained using a 20 $\mu$m Al foil (i.e., cathodic current collector) assembled in a conventional coin cell (half-cell). Third, the CV test series were conducted using 0.1 mm-thick Al foils (99.997%; Alfa Aesar) under the coin cell architecture. The prelithiation is achieved by first polarizing the cell at 10 mV versus Li/Li$^+$ for 15 min to achieve a homogenous nucleus distribution among the Al electrode surfaces.[8] The potential was then switched to a moderate level (150 mV vs Li/Li$^+$) to facilitate constant propagation of the phase boundary and to form a homogenous layer of $\beta$-LiAl covering the surface of the Al foil until the desired prelithiation depths are achieved.[8] For instance, a 20 $\mu$m prelithiation depth refers to 0.002 cm × 1 cm$^2$ × 2.7 g/cm$^3$ × 993 mA h/g = ~5.36 mA h/cm$^2$.

**Ex Situ XRD.** A deeply lithiated Al electrode underwent X-ray diffraction using a high-energy Rigaku SmartLab diffractometer equipped with a Mo anode tube. Such a Li−Al electrode was prepared by disassembling a Swagelok cell that had gone through a potentiostatic hold at 10 mV versus Li/Li$^+$ for 3 days and then sealing into Kapton tapes inside an argon-filled glovebox prior to the XRD test.

**In Situ Stress Measurement.** Cantilevers made of aluminum oxide with the size of 15 × 5 × 0.25 mm$^3$ are double-side polished prior to the similar physical vapour deposition processes described in a previous study.[9] The thickness of TiN (current collector) and Al (electrode material) for stress measurement are characterized to be ~160 and ~420 nm, respectively. The GCD tests were run for the in situ stress cell at a rate of C/10, determined by the total charge of the Al film. The in situ stress measurement was achieved using the method of substrate curvature. In a substrate-based model where a rigid interface exists, the volume expansion caused by Li insertion strains the substrate and results in compressive stresses. A homebuilt three-electrode cell and two-beam laser setup allowed simultaneous measurement of the curvature of the substrate. Once the lithiation starts, the bending of the alumina cantilever can be tracked in situ by recording the distance change between the two laser spots. It should be noted that the stress values are normalized to the initial Al film thickness, referring to the nominal stress, such that the thickness change during (de-)lithiation is not taken into consideration. In other words, the mechanical stress reported in this study is a product of stress−thickness over the initial thickness and can be quantified using the Stoney equation (details can be found elsewhere).[9]

**Cross-Sectional SEM.** The Swagelok cells that can be easily disassembled were used here. When the Al foil was lithiated/delithiated to the desired state of charge/discharge, the Swagelok cell was disassembled in an argon-filled glovebox. The partly lithiated/delithiated Al foils underwent a series of grinding processes using sandpapers from #1000 to #5000 to create a flat and smooth cross-section. A thick foil obtained from Alfa Aesar (99.9995%; 0.25 mm) was used to maximize the cross-sectional area. Electrochemically, the thick foils were lithiated using potentiostatic modes under a constant driving force. A specifically designed transfer system (Leica VCT100) allows for the immediate sample transfer from the glovebox to the SEM system (Zeiss Merlin) without exposure to air. SEM images were acquired at an acceleration voltage of 6 kV, using both a SE detector and a BSE detector, such that the three-dimensional (3D) morphology and the $\beta$ phase distribution can be clearly revealed.

**Full-Cell Performance Assessment.** A commercially available LFP cathode was purchased (1 mA h cm$^{-2}$; CUSTOMCELLS, Germany) and paired with the novel bilayer $\beta$-LiAl anode developed in this study. The cells were examined in a Swagelok-type cell ($\varnothing$ = 11 mm), using a porous polymer separator (Celgard, USA) and LiPF$_6$ electrolyte (1 M, EC/EMC 3:7 vol %). The current rate equivalent to C/10 (normalized to the LFP cathode; 0.1 mA cm$^{-2}$) with a voltage window between 2 and 3.7 V was used for cycling performance assessment.

## ■ RESULTS AND DISCUSSION

During the experimental design, we strategically focused on partial lithiation to circumvent any possible formations of Li-rich phases. While the $\alpha$ phase is present and overall $\alpha/\beta$ equilibrium is maintained, only $\beta$-LiAl is expected to form at relatively high potentials (>0.2 V $vs$ Li/Li$^+$; $i.e.$, lithiation plateau), although an overpotential is required to move the phase front. In this case, the Li solubility within the $\beta$-LiAl can be characterized and discussed in isolation.

**Solubility Range Characterized by Electrochemical Techniques.** Figure 1a shows a typical cyclic voltammogram of Al foils against Li metal obtained at a slow scan rate of 0.01 mV s$^{-1}$, covering a wide potential range from 1 to 0 V $versus$ Li/Li$^+$. The sharp peaks near 0.2 V (reduction) and 0.5 V (oxidation) depict the formation of $\beta$-LiAl and the reformation of the $\alpha$ phase, respectively. Apart from the reactions of alloying and dealloying, there is also a broad but weak peak at ~0.3 V (blue arrow) that was considered by Hudak $et$ $al.$ as "unexplained".[22] Furthermore, one can notice that the reduction current is almost zero prior to the lithiation peak while it does not go back to zero after the lithiation peak. Interestingly, the electrical charge integrated from the reduction current after the $\beta$-phase formation peak ($i.e.$, ~0.2 to 0 V; 0.826 mA h cm$^{-2}$) is the same as the amount integrated from the oxidation current prior to the delithiation peak ($i.e.$, 0 to ~0.4 V; 0.827 mA h cm$^{-2}$). This amount of reversible capacity is calculated to be around 18% as compared to the one contributed by $\alpha/\beta$ phase transformations ($i.e.$, ~4.7 and ~4.5 mA h cm$^{-2}$ integrated from the lithiation and the delithiation peak, respectively). Such an electrochemical indication suggests that some reversible reactions other than $\alpha/\beta$ equilibrium are probably occurring in these potential ranges, including (de-)lithiation of the SEI, formation of Li-rich phases, and (de-)saturation of the solubility range of the $\beta$-LiAl.

Electrochemical charge counting was used to examine the composition of lithiated Al (Li$_x$Al) at room temperature, focusing on the potential range for lithiation ($i.e.$, ~0.3 to 0 V). The thick Al foils used in this study are well suited for conducting such an experiment because the impact from
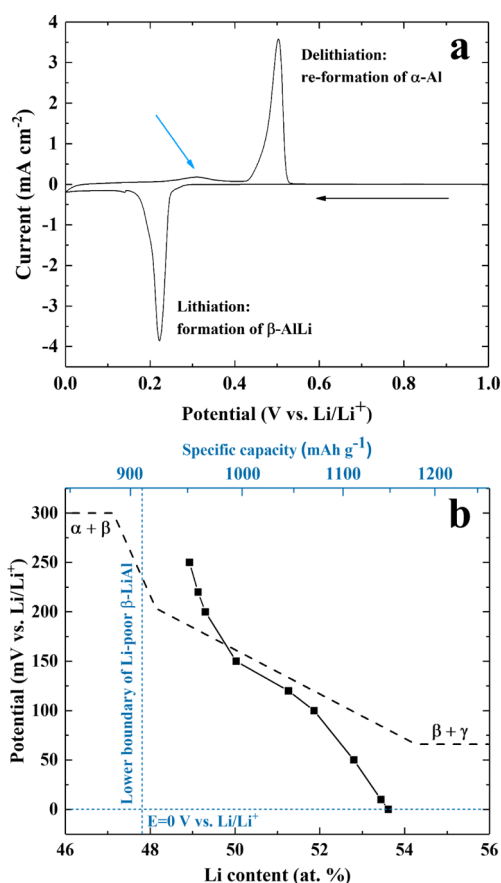


**Figure 1.** (a) Typical cyclic voltammogram of a 20 $\mu$m-thick Al foil obtained at a scan rate of 0.01 mV s$^{-1}$ (second cycle). The black and blue arrows indicate the scan direction and the unclarified delithiation bump, respectively. (b) Potentiostatic charge counting data obtained from 0.25 mm-thick Al foils covering a potential range from 250 to 0 mV $versus$ Li/Li$^+$ at room temperature, with the possible lower limit of the solubility range specified.

surface reactions, such as SEI formation and oxide lithiation, is negligible considering the overall thickness (0.25 mm, any native oxide layer is only present on the surface with a thickness on the nm scale). As can be seen from Figure 1b, potentiostatic charge counting indicates that the Li content in $\beta$-LiAl varies from 48.9 to 53.7 at % after the room-temperature lithiation within a potential range between 250 mV and 0 mV $versus$ Li/Li$^+$ for at least 96 h (250 mV for 120 h). A dashed line displays the Li solubility of the $\beta$ phase and the boundary of a Li-rich ($\gamma$) phase, previously determined by the coulometric titration method at 415 °C.[23,24] A sharp decrease in potential was observed by adding a small amount of Li on the Li-poor side at 415 °C, which corresponds to the large negative slope at low Li content we obtained at room temperature. On the Li-rich side, the $\beta$ and the $\gamma$ phase coexist at 415 °C, exhibiting a potential plateau at ~70 mV, for a Li content beyond ~54 at %. For our charge counting, no indication of the $\gamma$ phase can be seen from the phase diagram published in 1982.[16] Additionally, an XRD test has been performed for a deeply lithiated Al foil. The obtained diffractogram in Figure S1 only shows the $\beta$-LiAl peaks. Together, crystalline Li-rich phases higher than $\beta$-LiAl are either absent or minute in the fully lithiated foil samples ($i.e.$, amorphous phases cannot be excluded).[18] The present work focuses on cycling within the solubility range. However, the
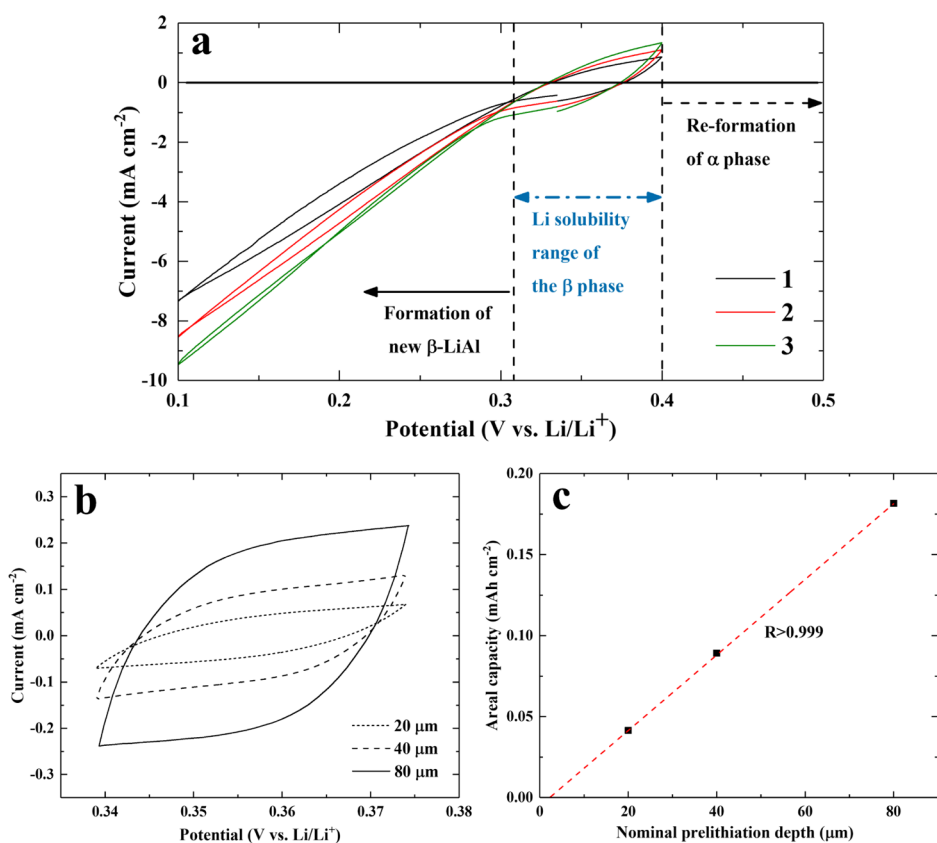
**Figure 2.** (a) CV scans between 0.4 and 0.1 V *versus* Li/Li$^+$ for the prelithiated 100 $\mu$m Al foils at a scan rate of 0.1 mV s$^{-1}$; the nominal prelithiation depth is 20 $\mu$m based on the calculation of electric charge. (b) CV cycling at 0.01 mV s$^{-1}$ within the determined Li solubility range while maintaining the $\beta$-LiAl structure for the Al foils with various nominal prelithiation depths. (c) Areal capacity integrated from the cyclic voltammograms as a function of the nominal prelithiation depth.

capacity that we determined for the formation of the $\beta$-LiAl phase, 1151.68 mA h g$^{-1}$, will be relevant for future work aiming at using the full capacity of the $\alpha/\beta$ phase transition: Instead of a theoretical capacity of 993 mA h g$^{-1}$ calculated for the ideal 50:50 composition (Li$_{1.000}$Al), a value of 1152 mA h g$^{-1}$ should be used as the theoretical capacity of the $\beta$ phase at room temperature, to account for the 53.7 at % of Li (Li$_{1.160}$Al).

It should be noted that the width of the actual Li solubility range of the $\beta$ phase is expected to be larger than the 4.8 at % determined by the potentiostatic charge counting performed during lithiation only: the range is expected to extend to lower concentrations during delithiation due to the overvoltage required to move the phase boundary (and to even lower concentrations if the nucleation of the $\alpha$ phase needs to take place). Clarification has been made by holding a fully lithiated Al foil at 375 mV *versus* Li/Li$^+$, where only desaturation of the $\beta$ phase is occurring (*i.e.*, no $\beta$ to $\alpha$ phase transformation). This lower boundary of the Li content in the $\beta$ phase is calculated to be 47.8 at % (Figure 1b) instead of the 48.9 at % obtained from the charge counting experiment at 250 mV, yielding a wider solubility range of 5.9 at % at room temperature. We note that this number has been examined by a control experiment that replicates the potentiostatic charge counting steps using a coin cell. The results are provided in Figure S2, in which consistency can be observed, supporting the reliability of the obtained data used for characterizing the solubility range. Still, the range is lower than the ~8 at % determined by the coulometric titration method at elevated temperature.[23] The

solid solution region is bounded by Li$_{1.160}$Al and Li$_{0.916}$Al, corresponding to specific capacities of 1152 and 910 mA h g$^{-1}$, respectively. Therefore, this solubility range should contribute to a specific capacity of ~242 mA h g$^{-1}$ (~21% of the full capacity), normalized to Al, in agreement with the integrated reversible capacity of the non-$\alpha/\beta$ phase transformation seen in CV.

The solubility range of a partly prelithiated Al foil is then characterized by a series of designated CV experiments. To begin with, the potential range is fixed to be between 0.4 and 0.1 V *versus* Li/Li$^+$ such that the formed $\beta$-LiAl is not delithiated beyond the solubility range and maintains its crystal structure. As illustrated in Figure 2a, when the potential is decreased from the equilibrium potential (~0.35 V *vs* Li/Li$^+$), a quasi-linear increase in the reduction current can be observed, agreeing with Geronov's rule that the speed of the phase boundary propagation rate should be linearly correlated with the driving force (*i.e.*, overpotential).[25] Here, the non-linear regime between ~0.32 V and 0.4 V *versus* Li/Li$^+$ should refer to the Li solubility range of $\beta$-LiAl, which is the only possible origin of reversible capacity. The lithiation kinetics generally follow the one-dimensional thickening process (*i.e.*, the geometry of the Deal–Grove model[8] but with propagation-limited kinetics) in the case of bulk Al foils. During the $\beta$-phase growth, a Li concentration gradient in the $\beta$ phase is required to keep the Li flux from the electrolyte to the phase interface and to enable continuous phase propagation. Therefore, the electrochemical driving force and the Li diffusion are of vital importance because of their strong effect on the phase

propagation and the Li concentration gradient, which determines the Li atom flux through the $\beta$-LiAl to the $\alpha/\beta$ phase interface. Accordingly, a narrower potential window and a slow scan rate should be chosen to ensure null propagation of the phase boundary and a sufficient time for Li to diffuse within the $\beta$-LiAl. The CV scan rate was initially set at 0.1 mV s$^{-1}$, but the obtained cyclic voltammograms in Figure S3 indicate that the (de-)saturation of $\beta$-LiAl seems to be limited by the Li diffusion.

Consequently, Figure 2b compares the cyclic voltammograms obtained at a 10 times slower scan rate (i.e., 0.01 mV s$^{-1}$) of the Al foil with various prelithiation depths. It can be seen that the deeper the prelithiation, the larger the CV area (i.e., capacity, energy stored, etc.), suggesting that the prelithiated $\beta$ phase is cycled within its solubility range. Otherwise, all cases would yield a similar CV shape if the currents were contributed by the propagation of the phase interface (i.e., growth of more $\beta$-LiAl). As shown in Figure 2c, although the areal capacities exhibit perfect linearity versus nominal lithiation depth, a value of $\sim$2 $\mu$m instead of the coordinate origin is achieved by extrapolating the linear fit toward the left. This observation is indicative of the SEI formation, and thus, the actual lithiation depth is smaller by a constant value, compared to the nominal one calculated from the electrical charge. Quantitatively, the capacity estimated from the Al foil with a nominal lithiation depth of 20 $\mu$m (0.041 mA h cm$^{-2}$) is slightly lower than a half and one-fourth of those from the ones with 40 $\mu$m (0.089 mA h cm$^{-2}$) and 80 $\mu$m (0.181 mA h cm$^{-2}$), respectively. If taking into consideration the electrical charge that is consumed in SEI formation, perfect twofold relationships among them can be expected.

**Solubility Range Characterized by *In Situ* Stress Measurement.** In addition to the electrochemical characterizations, in situ substrate curvature tests were also conducted using a cell that is designed to quantify mechanical changes in the active material during cycling.[26] Figure 3 shows a partial electrochemical cycle of such a setup. The cell was assembled using the as-sputtered Al thin film on a flat substrate as the working electrode and was held at 0.4 V versus Li/Li$^+$ at a constant temperature such that surface reactions were minimized in the higher−potential regime. With the initial

state defining the zero stress, SEI formation and oxides contribute to a less than 2 MPa (<5% of the maximum) nominal stress after 4 h when the potential is held at 400 mV versus Li/Li$^+$. Yet, it still takes $\sim$2 h for the Al film electrode to be nucleated, as indicated by the potential dip at $\sim$5.8 h (also described elsewhere).[27] This can be explained by the finite thickness of the Al thin film ($\sim$420 nm), of which the native oxide layer occupies several tens of nanometers. The oxide lithiation together with the initial SEI formation in the lower-potential regime should be responsible for this long nucleation time and a nominal stress level of $\sim$20 MPa. Once the nucleation of $\beta$-LiAl occurs, a nearly linear buildup of compressive stress with a higher slope is observed during lithiation. As seen from the corresponding GCD profile, the electrode potential never goes below 0.2 V versus Li/Li$^+$, supporting the conclusion that $\beta$-LiAl is the only lithiated phase here as Li-rich phases often require very low potentials and possibly high temperatures.[17]

When the Al film reaches the end of a partial lithiation of $\sim$40% (i.e., $\sim$4 h after nucleation), the lithiated $\beta$-LiAl should be saturated to some extent as overpotentials are often required to facilitate the propagation of the phase boundary. Moving to delithiation, a rapid increase in the stress toward a tensile state is observed as soon as the current direction is reversed. The Li concentration in the $\beta$ phase must approach its minimum to prompt the phase transition from $\beta$-LiAl to $\alpha$-Al. This sudden stress jump at the beginning of lithiation is likely a result of desaturating the solubility range in the formed $\beta$-LiAl as the overall volume change may strain the substrate more significantly than the two-phase coexistence where the stress is restricted to a volume near the $\alpha/\beta$ interface. The decrease in Li content from Li-rich $\beta$-LiAl to Li-poor $\beta$-LiAl shifts the lattice parameter by $\sim$0.03 Å, corresponding to a volume contraction of $\sim$1.4% and causing this substantial stress change.[10] This solubility feature was also acknowledged by a previous study but for a fully lithiated Al film instead of a partly lithiated one.[9] Interestingly, the stress data of the previous study are consistent with the $\beta$-LiAl of a partly lithiated solid Al film being (de-)saturated without propagating the phase boundary in this work. Subsequently, a nanoporous $\alpha$-Al matrix will be created by further removing the Li atoms, like other dealloying processes,[28] thereby giving a stable stress signal from 11 h. The second cycle of the stress cell in Figure S4 shows generally similar features but with a more pronounced linear buildup of the compressive stress during lithiation due to less pronounced surface reactions.

**Fabrication and Characterization of the Bilayer Al-Based Electrode.** If the cycling capacity is limited to the Li solubility range of the prelithiated $\beta$-LiAl layer on top of an Al foil, it may be conjectured that the $\alpha/\beta$ interface will not move during charge−discharge, leading to long-term cycling capabilities. To prove this theory, SEM images were taken to help observe a partially (de-)lithiated Al foil. The prelithiation is carried out by initiating the potential at 10 mV for 15 min to achieve a homogenous nucleus distribution covering the whole electrode surface[29] and then holding at 150 mV to allow one-dimensional phase boundary propagation until the amount of charge that is sufficient to lithiate a certain depth.[25]

Figure 4 provides the cross-sectional views of a partially lithiated Al foil with and without a tilting angle, where a darker color refers to $\beta$-LiAl due to its lower electron density, resulting in a smaller number of the backscattered electrons. Figure 4a visualizes that the $\beta$-LiAl layer homogeneously
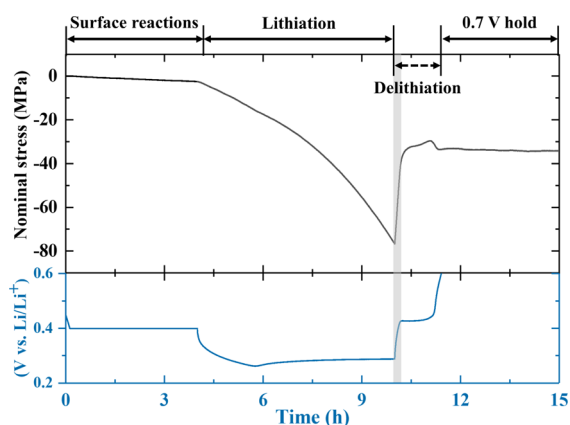


**Figure 3.** Nominal stress as a function of time coupled with potential responses for the initial cycle with a $\sim$40% lithiation depth. The shaded area refers to the solubility range of the $\beta$ phase. The same plot for the second cycle is provided in the Supporting Information as Figure S4.
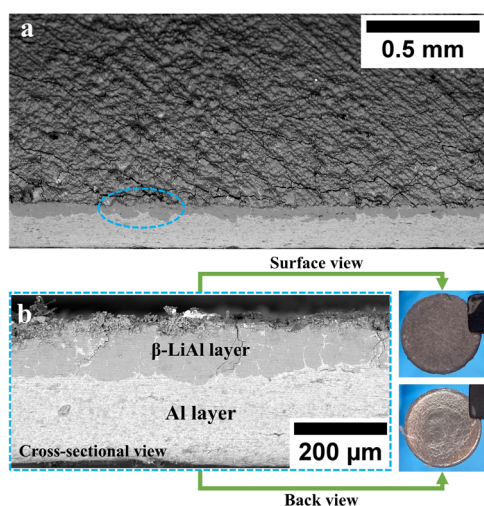
**Figure 4.** (a) SEM image taken for a partially lithiated Al foil using a 90° sample holder with a tilting angle of 45°, of which the cross-section is enlarged in (b) at a magnitude of 200×. The macroscopic views of the electrode surface and the backside are also shown.

covers the electrode surface while the cross-section (Figure 4b) exhibits a continuous, but imperfectly flat interface due to the random nucleation that is evidenced in a previous study.[8] From a macroscopic view, the surface of the Al foil electrode is covered with a layer of the dark $\beta$-LiAl while the backside exhibits the typical metallic features of aluminum.

These observations demonstrate the opportunity for solid-state bilayer Al-based anodes, that is, growing a continuous layer of $\beta$-LiAl (active material) on the surface of an Al foil (current collector). The idea here is to realize the Li solubility range without propagating the phase boundary and growing more $\beta$-LiAl at the consumption of $\alpha$-Al. From a thermodynamic point of view, one may argue that the inserted Li atoms might preferentially drive the phase interface to lithiate more fresh Al underneath when the two phases coexist rather than saturating the $\beta$ phase on top of the electrode. However, the formation of additional $\beta$-LiAl will be accompanied by intrinsic barriers (*e.g.,* mechanical strain, grain orientation, and nucleation),[30] causing overpotentials that largely prevent instantaneous phase transformation.

### Full Cell Demonstration of the Bilayer Al-Based Anode.

A full cell is used to assess its performance using such an Al-based anode and a commercially available LiFePO$_4$ cathode. The cell structure and the conditions are schematically illustrated in Figure 5a. The capacity contributed by the solubility range of the prelithiated $\beta$-LiAl is optimized to surpass the overall capacity of the cathode. The same Al foil (0.25 mm) is prelithiated to form the bilayer structure: The upper layer of 0.1 mm is transformed to $\beta$-LiAl and the remaining 0.15 mm functions as the current collector. The ideal capacity contributed by the solubility range is calculated to be ~6.5 mA h cm$^{-2}$ using a value of 1152 mA h g$^{-1}$ proposed in this study. However, the value can hardly be achieved because the overall $\alpha/\beta$ coexistence remains for the bilayer electrode, and any localized overlithiation or overpotential can result in the phase boundary movement. Therefore, we start with a high N/P ratio of 6.5, that is, the capacity of LFP cathodes is ~1 mA h cm$^{-2}$. This ensures that the $\alpha/\beta$ interface remains largely unperturbed.
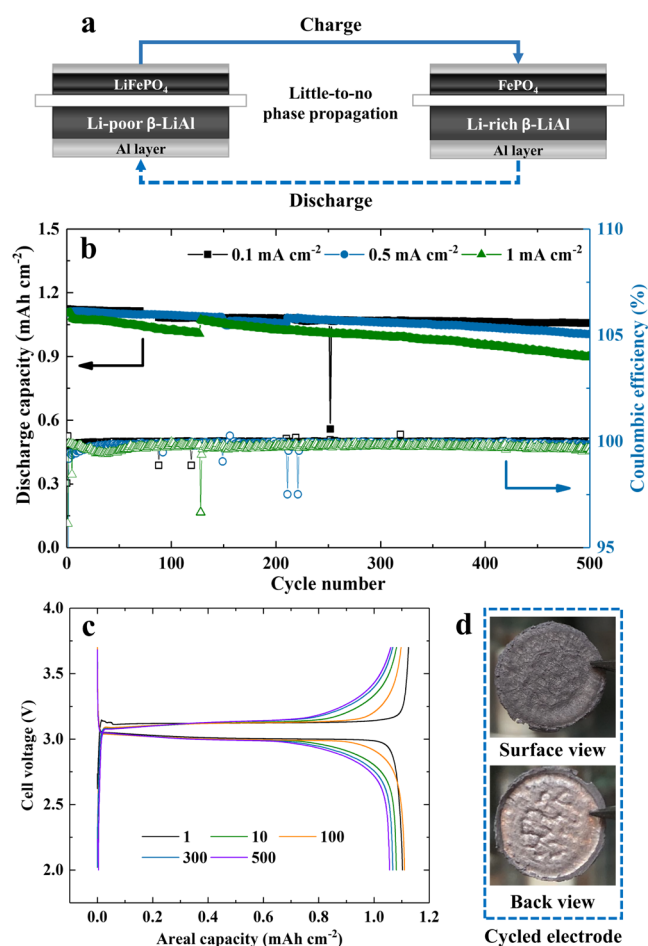


**Figure 5.** (a) Schematic illustrations of a novel full cell design using the $\beta$-LiAl grown on an Al foil as an anode and a commercial LFP cathode. (b) Cycling performance obtained at various current densities when the cathode capacity is below the one contributed by the solubility range of the $\beta$-LiAl anode. A control experiment using a thinner Al foil is provided in Figure S5. (c) GCD curves during the cycling at 0.1 mA cm$^{-2}$. (d) Macroscopic views of the electrode surface and the backside after cycling, in addition to the ones presented before.

As shown in Figure 5b, the assembled full cell exhibits excellent cycle lives with 95.8, 90.9, and 81.5% discharge capacity retention after 500 cycles for the current densities of 0.1, 0.5, and 1 mA cm$^{-2}$, respectively. At the rates slower than 0.5C, the capacity retention is equivalent to >99.99% (0.1 mA cm$^{-2}$) and >99.98% (0.5 mA cm$^{-2}$) per cycle. Although the cycling performance seems to be negatively affected by a faster rate, it already outperforms most of the commercially available batteries with ~99.96% cyclic capacity retention at 1 mA cm$^{-2}$. Some fluctuations in the Coulombic efficiency profile prior to 250 cycles are caused by unexpected interruptions (*e.g.*, laboratory power supply), which fortunately do not seem to affect the cycling performance of the cell. Finally, it should also be noted that the cell has been functioning well for more than 18 months at the time when this article is submitted.

Figure 5c depicts the GCD curves at increasing cycle numbers in Figure 5b, where similar features can be observed except the initial cycle. From these, the solubility range is only partly engaged in the first cycle, resulting in limited phase boundary movement. As cycling continues, the cell enters a balanced state where the solubility range of the $\beta$-LiAl layer

mostly contributes to the capacity of the anode with little-to-no phase propagation. This is consistent with the assumption that there should not be any significant changes in the Al electrode and $\beta$-LiAl is still intact during cycling. Figure 5d provides direct evidence in this regard: as observed, the bilayer structure of the Al electrode remains after around 250 cycles (backside is metallic Al), although the lateral expansion at the circumference and some creases can be observed on the backside due to the large stress change during (de-)saturation of $\beta$-LiAl.[9] When the cell is reassembled using the same electrodes, the cycling performance does not seem to be affected by the mechanical deformation, delivering the same capacity as before. Importantly, the previously mentioned benefits are achieved via a simple prelithiation step. Figure S6 further highlights the vital role of the prelithiation by showing the poor cycling performance obtained from the full cell with LFP versus unprelithiated Al foil.

Although the presented results already exhibit readiness in commercialization, it is relevant to question the high N/P ratio or the low volumetric capacity of $\beta$-LiAl on the Al electrode. Optimization efforts are required from an engineering point of view to explore the best proportion between the $\beta$-LiAl layer and the metallic Al layer and the N/P ratio. For instance, a quick demonstration is provided in the Supporting Information (Figure S5) that the concept is successful for commercially available Al foil (0.18 mm; Toyo Aluminum K.K.). Here, the prelithiation depth is performed in a different way: The upper layer of 0.06 mm is transformed to $\beta$-LiAl, and the remaining 0.12 mm functions as the current collector. Both layers are thinner than the ones used in Figure 5, yet the cycling performance is hardly affected (500 stable cycles) when pairing this electrode with the same LFP cathode. In this case, the capacity of the solubility range is calculated to be ~3.9 mA h cm$^{-2}$, giving a smaller N/P ratio of ~3.9 that can hopefully be further minimized.

## CONCLUSIONS AND PERSPECTIVES

Cumulatively, these results exhibit excellent prospects and readiness for commercialization because a simple rolling method for the prelithiation of Al and the processing of LiAl is available. Furthermore, these observations explain the origin of the anomalous success of some cells with Al anodes mentioned in the literature. For full cells where the capacity of the cathode is small compared to the capacity stemming from the Li solubility range in the $\beta$ phase, indefinite cycle life can be expected for the anode. Similarly, if the mismatch between the electrode capacities is small, then only minimal propagation of the $\beta$ phase is expected. When there is an excess of the $\alpha$ phase in the foil, the cell will be able to cycle for a very long time because the pristine $\alpha$ phase cannot be consumed by lithiation with the limited Li supply in the cathode. Of course, the influence of the mechanical strength of the pristine $\alpha$-Al underlayer merits continued investigation and optimization. Although the electrochemical formation of the $\alpha/\beta$ layered structure may be preferred experimentally due to the precise control of prelithiation depth, simple metallurgical bonding such as mechanical rolling may be an ideal way of forming such an anode.

LiAl is an attractive candidate for Li-based anodes in many applications, given its excellent cycling performance, low potential, and modest to high capacity figures—about 242 mA h g$_{Al}$$^{-1}$ for high cycling stability as suggested here, up to 1152 mA h/g$_{Al}$$^{-1}$ for few-cycle batteries. Furthermore,

considering the prospects for simple foil-based construction, the solid-state layered Al-based anode provides a low barrier to market entry if manufacturing, tooling, and labor costs are comprised. Even aside from a foil design (i.e., ≥0.1 mm), the metallurgical opportunities afforded by Al open up pathways for high-performance 3D architectures, as already indicated by novel IdEA platforms explored by others.[31] From the end-of-life perspective, a piece of metallic foil might offer alternative options for recyclers and waste processors who are concerned about the challenges of today's standard composite electrode designs and the mixture of materials therein.[32]

## ■ ASSOCIATED CONTENT

### ⓈⒾ Supporting Information

The Supporting Information is available free of charge at https://pubs.acs.org/doi/10.1021/acssuschemeng.1c07242.

> X-ray diffractogram of a deep lithiated Al foil; control experiment of charge counting; CV test series; in situ stress data; control experiment of cycling assessment; and cell performance of the LFP cathode versus pure Al foil (i.e., unprelithiated) anode (PDF)

## ■ AUTHOR INFORMATION

### Corresponding Author

**Steven T. Boles** − Department of Energy and Process Engineering, Norwegian University of Science and Technology, Trondheim 7491, Norway; ● orcid.org/0000-0003-1422-5529; Email: steven.boles@ntnu.no

### Authors

**Tianye Zheng** − Department of Electrical Engineering, The Hong Kong Polytechnic University, Kowloon 999077, Hong Kong; ● orcid.org/0000-0002-2281-9506

**Dominik Kramer** − Institute for Applied Materials, Karlsruhe Institute of Technology, Eggenstein-Leopoldshafen 76344, Germany

**Reiner Mönig** − Institute for Applied Materials, Karlsruhe Institute of Technology, Eggenstein-Leopoldshafen 76344, Germany; ● orcid.org/0000-0003-1048-9973

Complete contact information is available at:
https://pubs.acs.org/10.1021/acssuschemeng.1c07242

### Notes

The authors declare no competing financial interest.

## ■ ACKNOWLEDGMENTS

## ■ REFERENCES

(1) Rao, B. M. L.; Francis, R. W.; Christopher, H. A. Lithium-Aluminum Electrode. J. Electrochem. Soc. **1977**, 124, 1490−1492.

(2) Baranski, A. S.; Fawcett, W. R. The Formation of Lithium-Aluminum Alloys at an Aluminum Electrode in Propylene Carbonate. *J. Electrochem. Soc.* **1982**, *129*, 901−907.

(3) Jow, T. R.; Liang, C. C. Lithium-Aluminum Electrodes at Ambient Temperatures. *J. Electrochem. Soc.* **1982**, *129*, 1429−1434.

(4) Obrovac, M. N.; Chevrier, V. L. Alloy Negative Electrodes for Li-Ion Batteries. *Chem. Rev.* **2014**, *114*, 11444−11502.

(5) Kim, J. M.; Guccini, V.; Kim, D.; Oh, J.; Park, S.; Jeon, Y.; Hwang, T.; Salazar-Alvarez, G.; Piao, Y. A novel textile-like carbon wrapping for high-performance silicon anodes in lithium-ion batteries. *J. Mater. Chem. A* **2018**, *6*, 12475−12483.

(6) Tahmasebi, M. H.; Kramer, D.; Mönig, R.; Boles, S. T. Insights into Phase Transformations and Degradation Mechanisms in Aluminum Anodes for Lithium-Ion Batteries. *J. Electrochem. Soc.* **2019**, *166*, A5001−A5007.

(7) Huang, T. S.; Brittain, J. O. The mechanical behavior of $\beta$-LiAl. *Mater. Sci. Eng.* **1987**, *93*, 93−97.

(8) Zheng, T.; Kramer, D.; Tahmasebi, M. H.; Mönig, R.; Boles, S. T. Improvement of the Cycling Performance of Aluminum Anodes through Operando Light Microscopy and Kinetic Analysis. *ChemSusChem* **2020**, *13*, 974−985.

(9) Zheng, T.; Kramer, D.; Tahmasebi, M. H.; Mönig, R.; Boles, S. T. Exploring the Reversibility of Phase Transformations in Aluminum Anodes through Operando Light Microscopy and Stress Analysis. *ChemSusChem* **2020**, *13*, 5910−5920.

(10) Kishio, K.; Brittain, J. O. Defect structure of $\beta$-LiAl. *Phys. Chem. Solids* **1979**, *40*, 933−940.

(11) Boles, S. T.; Tahmasebi, M. H. Are Foils the Future of Anodes? *Joule* **2020**, *4*, 1342−1346.

(12) Gogotsi, Y.; Simon, P. True Performance Metrics in Electrochemical Energy Storage. *Science* **2011**, *334*, 917.

(13) Ryu, J.; Kang, J.; Kim, H.; Lee, J. H.; Lee, H.; Park, S. Electrolyte-mediated nanograin intermetallic formation enables superionic conduction and electrode stability in rechargeable batteries. *Energy Storage Mater.* **2020**, *33*, 164−172.

(14) Kim, Y.; Ha, K.-H.; Oh, S. M.; Lee, K. T. High-Capacity Anode Materials for Sodium-Ion Batteries. *Chem.—Eur. J.* **2014**, *20*, 11980−11992.

(15) Guidotti, R. A.; Masset, P. J. Thermally activated ("thermal") battery technology: Part IV. Anode materials. *J. Power Sources* **2008**, *183*, 388−398.

(16) McAlister, A. J. The Al−Li (Aluminum−Lithium) system. *Bull. Alloy Phase Diagrams* **1982**, *3*, 177−183.

(17) Ghavidel, M. Z.; Kupsta, M. R.; Le, J.; Feygin, E.; Espitia, A.; Fleischauer, M. D. Electrochemical Formation of Four Al-Li Phases ($\beta$-AlLi, $Al_2Li_3$, $AlLi_{2-x}$, $Al_4Li_9$) at Intermediate Temperatures. *J. Electrochem. Soc.* **2019**, *166*, A4034−A4040.

(18) Qin, B.; Diemant, T.; Zhang, H.; Hoefling, A.; Behm, R. J.; Tübke, J.; Varzi, A.; Passerini, S. Revisiting the Electrochemical Lithiation Mechanism of Aluminum and the Role of Li-rich Phases ($Li_{1+x}Al$) on Capacity Fading. *ChemSusChem* **2019**, *12*, 2609−2619.

(19) Ji, B.; Zhang, F.; Sheng, M.; Tong, X.; Tang, Y. A Novel and Generalized Lithium-Ion-Battery Configuration utilizing Al Foil as Both Anode and Current Collector for Enhanced Energy Density. *Adv. Mater.* **2017**, *29*, 1604219.

(20) Zhang, M.; Xiang, L.; Galluzzi, M.; Jiang, C.; Zhang, S.; Li, J.; Tang, Y. Uniform Distribution of Alloying/Dealloying Stress for High Structural Stability of an Al Anode in High-Areal-Density Lithium-Ion Batteries. *Adv. Mater.* **2019**, *31*, 1900826.

(21) Li, H.; Yamaguchi, T.; Matsumoto, S.; Hoshikawa, H.; Kumagai, T.; Okamoto, N. L.; Ichitsubo, T. Circumventing huge volume strain in alloy anodes of lithium batteries. *Nat. Commun.* **2020**, *11*, 1584.

(22) Hudak, N.; Huber, D. Nanostructured lithium-aluminum alloy electrodes for lithium-ion batteries. *ECS Trans.* **2011**, *33*, 1−13.

(23) Wen, C. J.; Boukamp, B. A.; Huggins, R. A.; Weppner, W. Thermodynamic and Mass Transport Properties of "LiAl". *J. Electrochem. Soc.* **1979**, *126*, 2258.

(24) Wen, C. J.; Weppner, W.; Boukamp, B. A.; Huggins, R. A. Electrochemical investigtion of solubility and chemical diffusion of lithium in aluminum. *Metall. Mater. Trans. B* **1980**, *11*, 131−137.

(25) Geronov, Y.; Zlatilova, P.; Staikov, G. The secondary lithium-aluminium electrode at room temperature. *J. Power Sources* **1984**, *12*, 155−165.

(26) Choi, Z.; Kramer, D.; Mönig, R. Correlation of stress and structural evolution in $Li_4Ti_5O_{12}$-based electrodes for lithium ion batteries. *J. Power Sources* **2013**, *240*, 245−251.

(27) Wang, C. Y.; Meng, Y. S.; Ceder, G.; Li, Y. Electrochemical Properties of Nanostructured $Al_{1-x}Cu_x$ Alloys as Anode Materials for Rechargeable Lithium-Ion Batteries. *J. Electrochem. Soc.* **2008**, *155*, A615−A622.

(28) Chen, Q.; Sieradzki, K. Spontaneous evolution of bicontinuous nanostructures in dealloyed Li-based systems. *Nat. Mater.* **2013**, *12*, 1102.

(29) Geronov, Y.; Zlatilova, P.; Staikov, G. Electrochemical nucleation and growth of $\beta$-Lial alloy in aprotic electrolyte solutions. *Electrochim. Acta* **1984**, *29*, 551−555.

(30) Zheng, T.; Wang, X.; Jain, E.; Kramer, D.; Münig, R.; Seita, M.; Boles, S. T. Granular phase transformation of polycrystalline aluminum during electrochemical lithiation. *Scr. Mater.* **2020**, *188*, 164−168.

(31) Heligman, B. T.; Kreder, K. J.; Manthiram, A. Zn-Sn Interdigitated Eutectic Alloy Anodes with High Volumetric Capacity for Lithium-Ion Batteries. *Joule* **2019**, *3*, 1051−1063.

(32) Heligman, B. T.; Manthiram, A. Elemental Foil Anodes for Lithium-Ion Batteries. *ACS Energy Lett.* **2021**, *6*, 2666−2672.

## ⧉ Recommended by ACS